Melt Crystallization for Paracetamol Polymorphism

Alexander G. Shtukenberg,[a]* Melissa Tan,[a] Leslie Vogt-Maranto,[b] Eric J. Chan,[b] Wenqian Xu,[c] Jingxiang Yang,[a] Mark E. Tuckerman,[bde] Chunhua T. Hu[a] and Bart Kahr[a]*

[a]Department of Chemistry and Molecular Design Institute, New York University, New York City, NY, 10003, USA

[b]Department of Chemistry, New York University, New York City, NY, 10003, USA

[c]X-ray Science Division, Advanced Photon Source, Argonne National Laboratory, Argonne, Illinois 60439, USA

[d]Courant Institute of Mathematical Science, New York University, New York City, NY, 10003, USA

[e]New York University-East China Normal University Center for Computational Chemistry at NYU Shanghai, 3663 Zhongshan Road North, Shanghai 200062, China

*Corresponding authors: A. G. Shtukenberg shtukenberg@mail.ru; Bart Kahr bart.kahr@nyu.edu.

ABSTRACT Polymorphism plays a crucial role in pharmaceutical formulations of paracetamol, one of the most commonly used analgesic and antipyretic drugs. Trimorphic paracetamol has been a model system for studying transformations among phases of molecular crystalline materials. During crystallization from the melt and the glass above 0 °C, three new polymorphs of paracetamol (*N*-acetyl-*para*-aminophenol or acetaminophen) were discovered, doubling the number of known ambient forms. The crystal structure of one of these was solved using a combination of powder X-ray diffraction and computational techniques. Analysis of growth kinetics revealed an anomalous temperature dependence near the glass transition: as temperature decreases, growth rate increases. This rare and poorly understood phenomenon is commonly identified as the glass to crystal (GC) growth mode. In addition, two polymorphs, displayed optical evidence of helicoidal morphologies, a characteristic of at least 25% of molecular crystals that has been resistant to a universal explanation.

INTRODUCTION

Melt crystallization pairs high driving force with low nucleation and growth rates to unlock regions of the potential energy landscape inaccessible through solution growth. This benefits the analysis of molecular crystals, particularly for the development of active pharmaceutical ingredients (APIs), by clarifying fundamental aspects of crystal growth and providing an additional powerful option for polymorph screening.[1] In recent years we have applied melt crystallization to the study of several important materials, including testosterone propionate,[2] resorcinol,[3] aspirin,[4] coumarin,[5]

and DDT.[6] In each case, our research has led to the identification of new polymorphs. Here, we extend this approach to paracetamol.

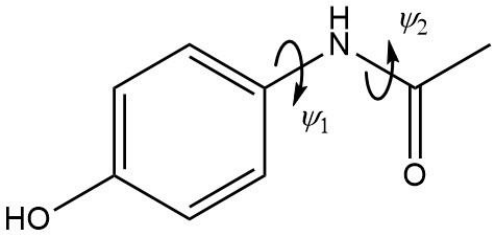

Scheme 1. Paracetamol, $C_8H_9NO_2$, MW = 151.16 g/mol

Paracetamol (*N*-acetyl-*para*-aminophenol or acetaminophen, CAS # 103-90-2, Scheme 1) is a common analgesic and antipyretic drug. Prior to our work, six polymorphs of paracetamol were known: three ambient (**I**, **II**, and **III**),[7,8,9] two high-pressure (**IV** and **V**),[10] and one low temperature phase (**III-m**, which we have renamed **VI**).[11] Of these, **I**, **II**, **III**, and **VI** have solved structures.

In contrast to many molecular compounds, melt crystallization of paracetamol is well studied. Form **III** was obtained from the melt[12] and its crystal structure was subsequently solved with powder diffraction data.[9] Recently, **III** was observed to undergo a reversible transition to **VI** between -103 and -53 °C.[11] Although details of phase relationships are inconsistent between publications, most indicate that **III** crystallizes from the melt between 54 and 85 °C and converts to **II** between 70 and 120 °C.[9,12,13,14,15,16,17,18] Both **I** and **II** can crystallize from 25-75 °C, especially if the sample is exposed to air.[12,13,19,20] Paracetamol **II** is relatively stable at ambient pressure but can undergo transformation (**II→I**) over a wide range of temperatures.[19,20,21] Nucleation of paracetamol **I** from the melt was also studied computationally.[22]

In this paper, we report on the growth phenomena, kinetics, polymorphism, and phase transformations of paracetamol crystallized from the melt/glass above 0 °C. We relied on hot stage polarized light microscopy for visualization of growth morphologies and phase transformations. The identities of the polymorphs, revealed based on morphology and crystal optical signatures, were then confirmed using powder X-ray diffraction and Raman spectroscopy. This led to the observation that two phases of paracetamol (**I** and **III**) can form twisted crystals from the melt and to the discovery of three new ambient polymorphs (**VII**, **VIII**, and **IX**). The crystal structure of **VII** was solved using a combination of powder X-ray diffraction and computational techniques. In addition, crystallization and transformation pathways in the range from 0 to 170 °C were

analyzed and refined, leading to the discovery of non-monotonic growth rate behavior as a function of temperature around glass transition temperature that corresponds to the glass-to-crystal growth (GC) mode.

POLYMORPHISM AND MORPHOLOGY

Crystallization and phase transformation phenomena observed in paracetamol grown from the melt and glass are summarized in Table 1 and Figures 1, 2, and 3. Unless otherwise stated, observations correspond to interior regions of the film isolated from direct contact with air.

Table 1. Crystallization from melt/glass and phase transformations in paracetamol polymorphs in the absence of direct contact with the air.

Temperature range, °C	Crystallization			Transformation[a]	
	via nucleation in melt/glass	via cross nucleation	via growth front advancement	via growth front advancement	via nucleation
$T_{m,II} \approx 157 < T < T_{m,I} \approx 169$	**I**		**I**		
$T_{m,III} \approx 143 < T < T_{m,II} \approx 157$	**I**		**I, II**	**II→I**	
$T_{m,VI} \approx 133 < T < T_{m,III} \approx 143$	**I**	**II** on **III**	**I, II**	**II→I** **III→I, II**	 **III→II**
$\approx 110 < T < T_{m,VI} \approx 133$	**I**	**II** on **III**	**I, II**	**II→I** **III→I, II** **VII→I**	 **III→II** **VII→I**
$T_g \approx 25 < T < \approx 110$	**I, III, VII, VIII, IX**	**III** on **II**	**I, III, VII, VIII, IX**	**II→I** **III→I, II** **VII→I, II** **VIII→II**[b] **IX→I, II**,[c] **III, VII**	**IX→II**
$8 < T < T_g \approx 25$	**II**	**II** on **III**	**I, II, VII**		

[a]Rates detectable within 1 hour if temperature is above 100 °C; after a few hours if temperature is between 30 and 100 °C, and within a week if temperature is below 30 °C. (See temperatures in the leftmost column).
[b]**VIII→II** even if **VIII** is in contact with **III**.
[c]Sometimes **IX→II** even if **IX** is in contact with **III**.

Paracetamol **I** can grow throughout the temperature range studied. Above 90 °C, **I** occasionally nucleates at the center of the sample. As the temperature decreases, nucleation becomes confined to slide edges. **II** and **III** do not crystallize simultaneously at any temperature. Above *ca*. 110 °C, **III** ceases to grow and is replaced by **II** via cross nucleation (Figure 1h), initiating an unrelenting solid-state transformation from **III→II**. The growth of **III** is similarly arrested below the glass transition temperature (T_g = 25.2 °C as determined for quench cooled samples[13]). Although spherulites of **III** crystallized at higher temperatures can persist below T_g, their transformation is inevitable as **II** begins to nucleate in the glass and at the interface of **III** (Figure 1j, 2f). Between T_g and *ca*. 110 °C, smooth spherulites of **III**, displaying second to third order interference colors, dominate the melt. Although **II** can exist for weeks at these conditions, it cannot grow. Rather, **III**

begins to crystallize at the interface between **II** and the melt via cross nucleation. This is remarkable because **II** is more stable than **III** throughout the temperature range analyzed and because **III** eventually converts to **II** (Figure 1j). In general, our results agree with data in the literature,[12,13,14,15,16,17] however, although **III** was previously reported to crystallize between 54 and 85 °C, we observed its nucleation and growth between the T_g and *ca*. 110 °C, with the highest nucleation rates around 50 °C.

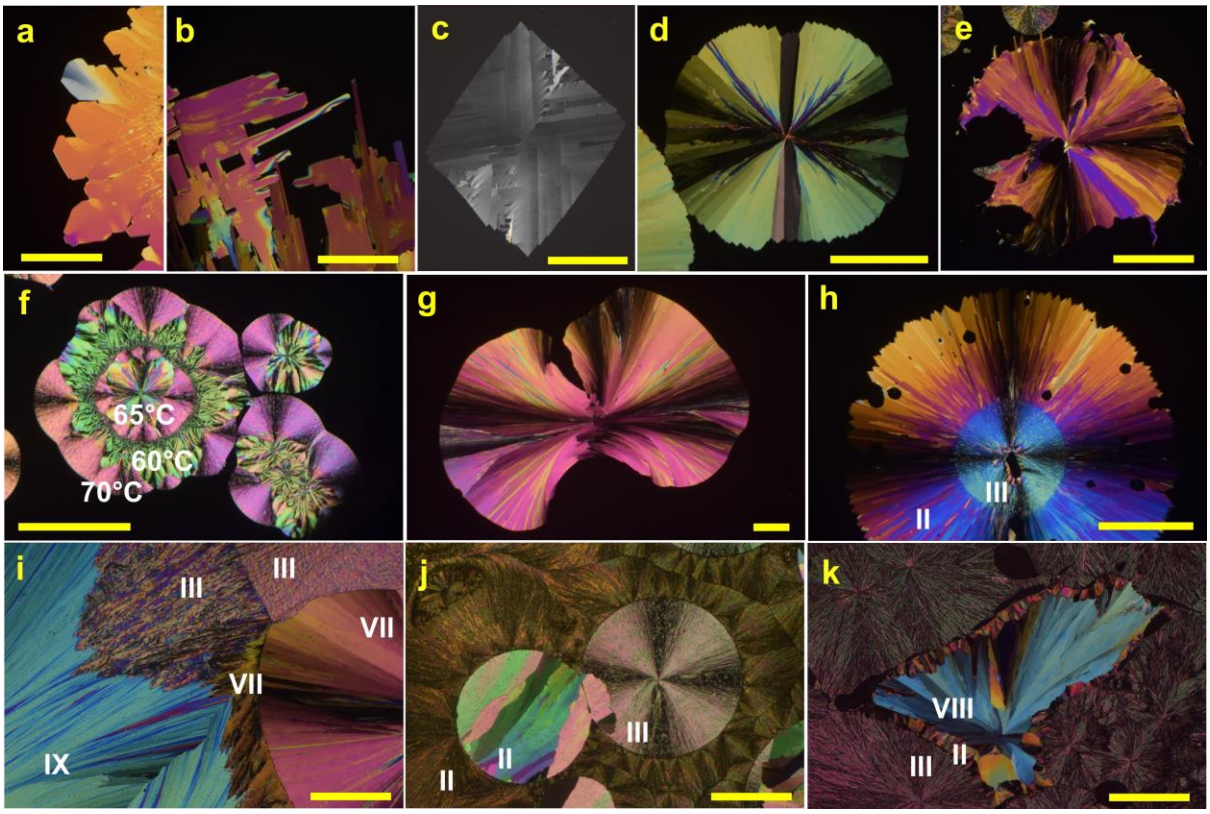

Figure 1. Polarized light optical micrographs of paracetamol polymorphs; polarizers are crossed for all images. (a) Crystals of **I** growing from the melt at 165 °C. (b) Crystals of **II** growing at 154 °C. (c) A branched crystal of **VII** growing at 65 °C viewed approximately along *a* direction (see section on crystal structure below). (d) A spherulite of **VII** growing at 65 °C. (e) A spherulite of **VIII** crystallized at 55-65 °C; the edges were grown at 45 °C. (f) Spherulites of **III** at different temperatures: purple center at 65 °C; thin darker layer surrounding at 50 °C; needles with green interference colors at 60 °C; and the outermost purple part at 70 °C. (g) A spherulite of **IX** growing at 65 °C. (h) A spherulite of **III** initially grown at 60 °C before raising the temperature to 120 °C. The needles grown at high temperature are **II**, while the small area at the center is **III** (grown at low temperature) transforming into **II**. (i) Phase transformations of **IX** in contact with **III** and **VII** at 65 °C. (j) Spherulites of **III** formed at 65 °C were stored at ≈23 °C. Within a couple weeks, spherulites of **II** nucleated in the glass and on the surface of **III**, prompting the transformation of **III** into **II**. (k) A spherulite of **VIII** surrounded by spherulites of **III** after crystallization at ≈50 °C. Transformation **VIII→II** has started at the interface between **III** and **VIII**. The scale bar is 500 μm for all images except (c), for which it is 200 μm.

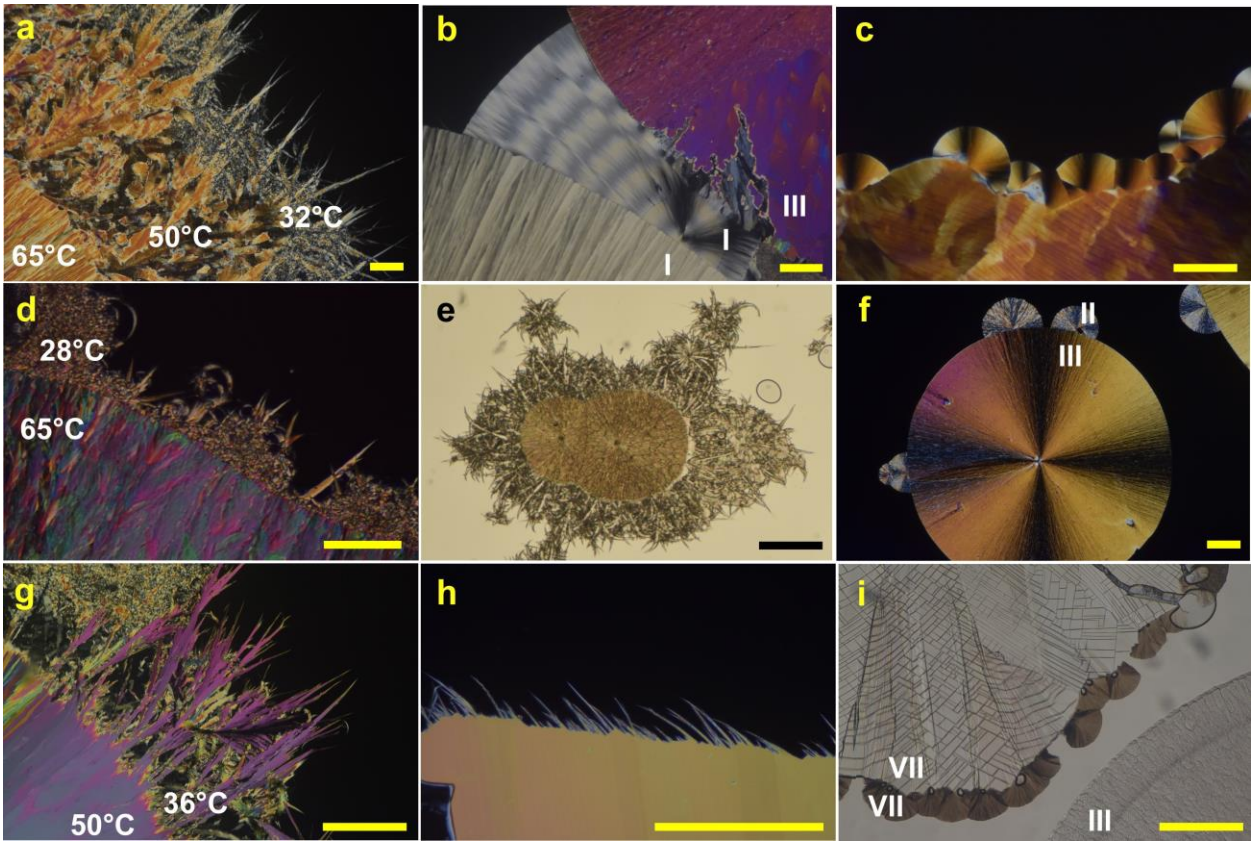

Figure 2. Polarized light micrographs of paracetamol crystallized near the glass transition temperature, T_g. Polarizers are crossed for all images except (e) and (i). (a) A compact spherulite of **I** becoming filamentous as temperature approaches T_g (growth temperatures in white). (b) A banded spherulite of **I** forming at 20 °C between compact spherulites of **I** (below) and **III** (above) that crystallized at *ca*. 65 °C. (c) Compact spherulites of **I** forming at 8 °C on the surface of **I** crystallized at ~60 °C. (d) A compact spherulite of **III** becoming filamentous as temperature decreased from 65 to 28 °C. (e) Cross nucleation of needle-like crystals of **III** on the surface of **II** at 35 °C. The spherulites of **II** were grown at ~23 °C. (f) Cross nucleation of compact spherulites of **II** on the surface of **III** at ~23 °C. The spherulites of **III** were grown at 65 °C. (g) and (h) Compact spherulites of **VII** becoming filamentous as temperature decreased from 50 to 36 °C and from 65 to 28 °C, respectively. (i) Compact spherulites of **VII** forming at 20 °C on the surface of **VII** crystallized at 65 °C. The scale bar is 200 μm for all images except (c) and (d), for which it is 50 μm.

Three new minor phases (**VII**, **VIII**, and **IX)** were observed between *ca*. 50 and 80 °C. Their presence was signaled by diverse polycrystalline patterns grown from the melt. While the differences in these micrographs may be hard to see to the inexperienced eye, parsing such subtleties is central to the identification of new polymorphs. For this reason, a brief discussion on distinguishing between structurally distinct phases with polarized light is presented here (Table 2). In plane polarized light, spherulites of **VII** are easily distinguished from **I**, **II**, **III**, **VIII**, and **IX** by the emergence of a network of cracks (Figure 2i). Sometimes, **VII** will grow as a single crystalline domain with nearly square dimensions and very low birefringence (Figure 1c). More often,

however, this metastable phase nucleates from a single point and grows as a smooth spherulite with some areas displaying a coarser texture with interference colors that range from blacks to light greys. In contrast to low-birefringent single crystallite domains, areas of **VII** that grow as a spherulite exhibit second to third order interference colors. Notably, the interface between spherulites of **VII** and the melt or glass phase is always jagged.

Paracetamol **VIII** crystallizes infrequently. Its optical signatures are similar to **VII**, but it exhibits more homogeneous birefringence with lower average birefringence and without areas of very low birefringence. **IX** is easily identified from other polymorphs by its high growth rate, unique morphology, and rapid transformation. After nucleating, **IX** grows as a double-leaf spherulite with second order interference colors visible between crossed polarizers (Figure 1g). In contrast to **VII** and **VIII**, the interface between **IX** and the melt or glass is always smooth.

Between *ca*. 50 and 80 °C **VII, VIII,** and **IX** can nucleate, grow, and remain relatively stable. Indeed, these metastable phases were observed to crystallize up to *ca*. 110 °C (Figure 3b); above this temperature, however, polymorph conversion becomes too fast. These phases do not form at high relative humidity, RH > 40 %. Under ideal conditions, RH < 30 % and 50 - 70 °C, **VII** composes *ca*. 2-5 % of total number of nuclei, while **IX** nucleates less frequently with < 1 %, and **VIII** is the rarest polymorph having only been observed three times. The percentage of **VII** and **IX** can be increased if a hydrophobic surface (Teflon coated glass) is used, but the nucleation of these forms is still inconsistent.

Near room temperature, spherulites of **VII** and **VIII** can remain intact for several weeks if isolated by the glass matrix. In contrast, **IX** transforms within a couple of days. Form **VII** does not undergo conversion if it is next to **III** or **II,** but can easily convert to **I** if it is in direct contact with **I**. If crystallites of **IX** collide with **I**, **II**, **III**, or **VII**, they start to convert to the more stable phase (Figure 1g,i,k). Sometimes, collision of **IX** with **III** produces **II**. This transformation processes take several minutes at ~70 °C or a few days at room temperature.

If the melt is exposed to air, paracetamol crystallizes within minutes by nucleation and growth of **I** and **II**. At room temperature, **II** remains stable for several weeks or longer. In contrast, **III** coverts to **II** and **VII** converts to **I** within minutes to hours, while **VIII** and **IX** convert to **II** within a few minutes. The transformation rate can be reduced dramatically under vacuum, as for **III** which remains stable for many hours.[9] The **IX→II** transformation is slow (on the order of a few hours) at room temperature under dry nitrogen, however, at ambient conditions, a powder sample of **IX**

converts to a mixture of **I** and **II** almost instantaneously. For samples prepared between glass slides, edges exposed to air and composed by the melt, glass, **III**, **VII**, or **IX** serve as a nucleation site for **I** and **II**. The transformation front quickly (mm/day to mm/several weeks depending on relative humidity) propagates inside the film and results in fast conversion into **I** and **II**.

Measurement of melting points for **VII**, **VIII**, and **IX** by differential scanning calorimetry (DSC) was not possible due to fast polymorph conversion. The melting points of **VII** and **IX**, T_m = 131.5(2) and 100(2) °C, respectively, were determined with a hot stage. These values are lower than T_m of **I** (169 °C), **II** (157 °C), and **III** (143 °C)[13,23] and suggest the following free energy ranking: **I** < **II** < **III** < **VII** < **IX**. This order is corroborated by polymorph conversion data (Table 1, Figure 1g,i). The rapid transformation of **VIII** prevented the identification of its melting point. However, from polymorph conversion (Table 1, Figure 1k) and growth kinetics (Figure 3b) we conclude that **III** < **VIII** < **IX**. Nevertheless, the relative stability of **VIII** *vs*. **VII** remains unknown.

The micro-Raman spectra of paracetamol polymorphs are similar but show distinct signatures (Figure 4). They are also similar to the published spectra[17,20,24,25,26] but sometimes differ in fine features, perhaps because of differences in crystal orientations.

Table 2. Morphologies and optical signatures of paracetamol polymorphs formed between 50 and 90 °C observed with a polarized light microscope.

Polymorph	Morphology	Spherulite/melt interface	Interference colors	Optic sign
I	Fine spherulite, birefringence can vary strongly for neighboring fibers	Smooth	1st order	+
II	Does not grow in this temperature range	Smooth	2nd order	-
III	Fine spherulite with homogeneous birefringence	Smooth	2nd to 3rd order	-
VII	Coarse spherulite with domains of very low birefringence	Saw tooth	2nd to 3rd order, some areas 1st order	-
VIII	Coarse spherulite	Irregular	2nd order	n/d
IX	Fine spherulite with a double leaf core	Smooth	2nd order	-

Spherulite is considered fine if it is hard to distinguish individual fibers, otherwise spherulite is coarse.[27] n/d – not determined.

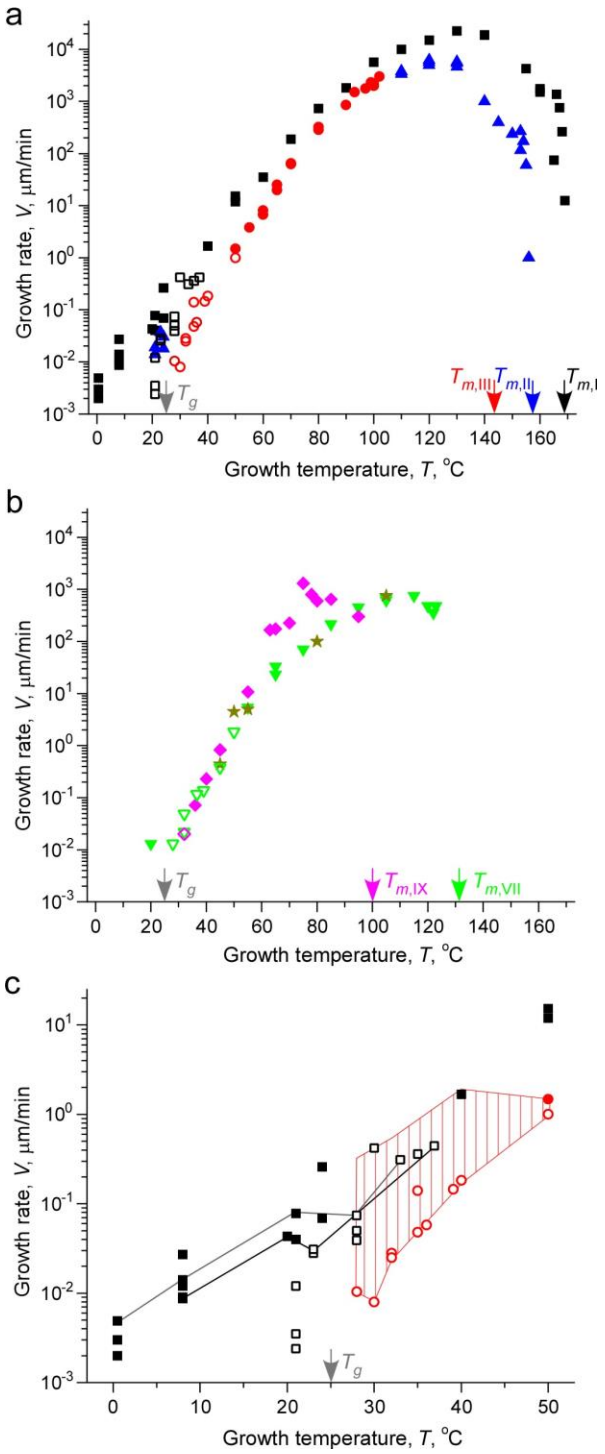

Figure 3. Growth rate of paracetamol polymorphs based on front advancement measured on a hot stage polarized light microscope. (a) **I** - black squares; **II** – blue triangles; **III** - red circles. (b) **VII** – green triangles; **VIII** – brown stars; **IX** – magenta diamonds. (c) A part of panel (a) with data on **I** and **III** near the glass transition temperature, T_g. Black and grey lines connect measurements performed for the same areas of the sample, respectively. The red hatched area corresponds to growth rates of Form **III** needles: the lower boundary corresponds to the majority of needles and the upper boundary corresponds to the fastest needles. In all panels, solid symbols represent compact growth fronts while open symbols indicate needle growth.

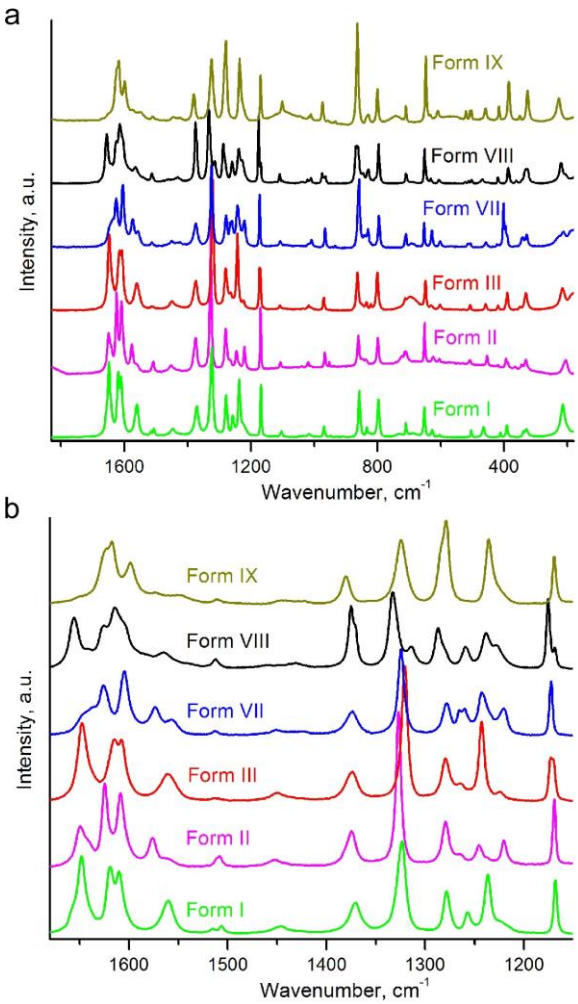

Figure 4. Raman spectra of paracetamol polymorphs. (b) Portion of (a) emphasizing differences.

GROWTH KINETICS

Growth rates of all polymorphs follow typical behavior with the maximum achieved at intermediate supercoolings, $\Delta T = T_m - T$ (Figure 3a,b). Growth of **I** is faster than all other polymorphs except for the least stable, **IX**, between 60 and 80 °C (Figure 5).

As with other materials crystallized from the melt,[27] **I** and **II** form branched crystals (Figure 1a,b) near T_m (for other polymorphs, observations of growth front propagation near T_m were impossible due to the fast conversion), while at lower temperatures all polymorphs (**I**, **II**, **III**, **VII**, **VIII**, and **IX**) develop as compact spherulites (Figure 1d-k). As temperature approaches T_g, spherulites of **I**, **III**, **VII**, **VIII**, and **IX** lose their compact morphology and grow as isolated needles (Figure 2a,d,e,g,h, 3). This behavior is also typical for crystallization around T_g.[2,28,29]

At temperatures just below T_g, **I** can grow as compact spherulites or needles (Figure 2i, 3a,c). For the same temperature, the growth rate, V, of compact spherulites is larger than that of needles. This growth acceleration at decreasing temperature is easy to follow in Figure 3c, where lines connect points measured at the same locations for different temperatures. The change in morphology from needles to compact spherulites results in an estimated growth rate acceleration of two to four times. Similarly, a growth acceleration of *ca*. five times was recorded for **VII**.

Needles of **I** grown near or above T_g were replaced by compact spherulites when the temperature decreased several degrees below T_g (Figure 2b,c, 3b). This abrupt change in growth morphology and kinetics near T_g may be indicative of the so-called glass-to-crystal (GC) growth mode, a phenomenon observed in fewer than 20 compounds so far.[2,28,29,30,31] GC growth is characterized by a significantly larger growth rate (up to 10^4 times) near T_g that outpaces growth rates predicted by diffusion. In paracetamol, this acceleration is modest. The largest enhancement attributed to the GC growth mode ($V_{max} \approx 0.1$ and 0.01 μm/min for **I** and **VII**, respectively) corresponds to the smallest absolute growth rates among all compounds exhibiting GC growth. The temperature of the GC mode onset, T_{GC}, is also comparatively small with $T_{GC}/T_g \approx 0.985$ fitting well to the empirical correlation established between these two values.[2]

Below T_g, **III** cedes growth to compact spherulites of **II** accompanied by a *ca*. ten-fold increase in growth rate (Figure 2f, 3a) reversing the cross nucleation of **II→III** observed around 110 °C. **II** is thermodynamically more stable than **III** at all temperatures; its curious disappearance and reappearance as the temperature approaches T_g is a consequence of kinetic factors and growth rates. While the apparent growth rate enhancement near T_g is tempting to identify as GC growth, we do not label as such since the correlated change in phase complicates the identification. Above T_g most needles of **III** have comparable growth rates and eventually form coarse spherulites. Some needles, however, can grow more than 30 times faster than others (Figure 3c, 6b,c,e), again signaling possible GC growth.[28,29]

The mechanism of the GC growth mode is still poorly understood. Although several hypotheses have been proposed, none have successfully accounted for all experimental observations so far.[29] The most plausible explanation[32] relies on the fact that crystals are typically denser than the glass. Microfractures produced by crystallization enable a faster glassy state transport along fractured surfaces than diffusional transport in the bulk, accelerating the overall

growth rate. As temperature increases, fracture formation is replaced by viscous flow and growth is controlled by the slower volume diffusion.

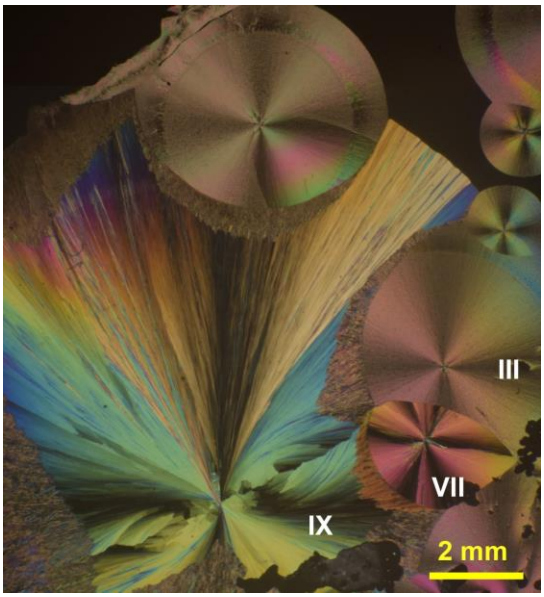

Figure 5. Polarized light micrograph of paracetamol polymorphs formed at 65 °C between crossed polarizers. Most of the area is occupied by a large spherulite of **IX**. Fast polymorph conversion is readily apparent at boundaries where **IX** is in contact with other forms. Figure 1i is a fragment of this image.

CRYSTAL TWISTING

After recording observations for 406 compounds, Bernauer concluded that roughly one in four molecular crystals grows as a mesoscopic helix from the melt.[33] Among the six ambient paracetamol polymorphs, we observed that two can twist (**I** and **III** in Figures 2b, 6), roughly matching Bernauer's prediction. The mechanism responsible for the formation of twisted crystals is a long-standing puzzle that has been a focus of our group.[34,35,36]

Compact spherulites of **I** grown at 20-21 °C, slightly below T_g, display optical banding that is a hallmark of twisting (Figure 2b).[33,34,35] The sample was measured with a Mueller matrix imaging polarimeter (550 nm, orthoscopic transmission) and the linear birefringence (|LB|) was recovered by analytic inversion (Figure 6f,g).[37] The oscillations in |LB| are clear evidence of rhythmic evolutions in the refractivity along the radial direction of the needle. Interestingly, neither compact polymorphs of **I** grown above (Figure 2a,b) or below (Figure 2c) this temperature, nor needles of **I** (Figure 2a), are twisted. This observation is consistent with testosterone propionate[2] and *o*-terphenyl,[28] which only twist in the GC growth mode.

Paracetamol **III** forms isolated needles between T_g and ~50 °C (Figure 3). Most of these needles are short and narrow in width as they grow, with tips that are often curved but not twisted (Figure 2d,e). Twisting generally emerges in needles with high length-to-width aspect ratios (Figure 6c,e) and occasionally manifests itself in banded spherulites (Figure 6d). In most twisted crystals, a larger cross section is associated with a smaller twist intensity: [34,38] this is not the case for paracetamol **III**. The twist intensity and cross-sectional area appear independent from one another (Figure 6b,c,e).

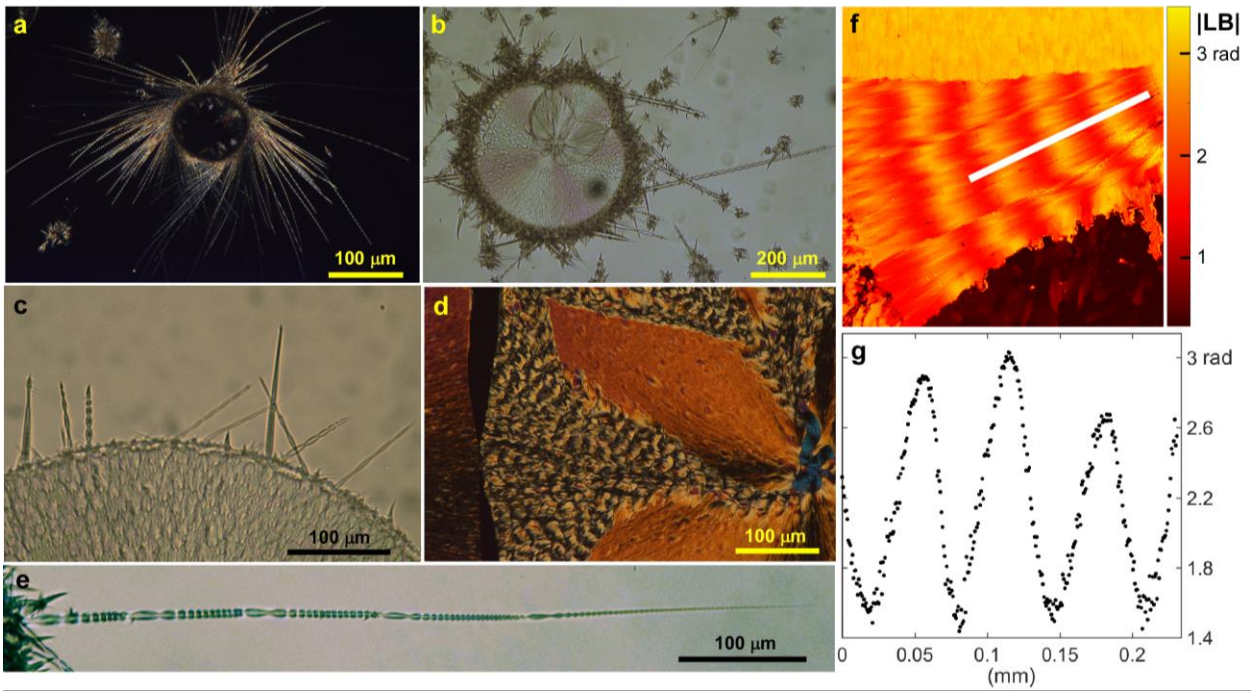

Figure 6. Twisted needle-like crystals of **III** grown at 26 °C (a), 35 °C (b), 36 °C (c) and 32 °C (e) viewed with a polarized light microscope. Note that a long twisted needle in (c, e) is much longer than other needles visible at the left hand side of the image. (d) Banded areas in a spherulite of **III** grown at 65 °C. (f) A false color image of oscillations in linear birefringence, an indication of rhythmically evolving refractivity, observed in a smooth spherulite of **I** (see Figure 2b). (g) Retardance measured along white line in (f).

PARACETAMOL VII CRYSTAL STRUCTURE

After several preliminary experiments performed on a Bruker AXS D8 DISCOVER GADDS microdiffractometer, synchrotron powder diffraction data for **VII** were collected on the 17-BM beamline (λ = 0.45457 Å) at the Advanced Photon Source (APS), Argonne National Laboratory at 200 K. The lattice constants were determined with the indexing software McMaille v3.04[39] as orthorhombic with a = 16.8444(2), b = 9.4822(1), c = 9.1419(1) Å, V = 1460.15(2) Å^3. This produced an excellent Pawley fit with R_p = 1.06, R_{wp} = 1.42, R_{exp} = 2.62 %. We identified four

*Pna*2$_1$ structures from the list of paracetamol forms predicted by Neumann and Perrin[40] with cell vectors and calculated PXRD patterns similar to the observed data. For the structure with the lowest energy of these candidates, structure_9, we combined the reported fractional coordinates with lattice constants and profile parameters from our best Pawley fit to obtain R_{wp} = 3.75 % for paracetamol **VII** without further refinement. The three other candidate structures, structure_11, structure_13, and structure_15, were analyzed in the same way, resulting in R_{wp} = 6.99 %, 9.68 %, and 10.84 %, respectively.

As comprehensive crystal structure prediction lists are not routinely available for all compounds, we chose to solve the structure directly from the powder data. Using the lattice constants determined above, molecules in the asymmetric unit were defined as rigid bodies and a structure solution was attempted with the simulated annealing procedure implemented in Bruker TOPAS 4.[41] The initial Pawley fit analysis suggested that space groups *P*2$_1$2$_1$2$_1$, *P*2$_1$2$_1$2, and *P*222$_1$ were likely candidates. The best match from the simulated annealing procedure using these space groups provided R_{wp} = 10.3 % fit for the *P*222$_1$ structure.

To check the packing options generated by simulated annealing, the energy was calculated using the general Amber force field (GAFF)[42] in the UPACK software package.[43] The atomic coordinates were relaxed within the observed unit cell and space group symmetries. For the *P*2$_1$2$_1$2$_1$, *P*2$_1$2$_1$2, *P*22$_1$2$_1$, and *P*222$_1$ TOPAS-refined structures, the calculated lattice energy was more than 10 kJ/mol higher than **I**. However, when the symmetry requirements were removed, geometry optimization of the *P*1 representation resulted in the *P*2$_1$2$_1$2 cell transforming into a *Pna*2$_1$ cell almost 10 kJ/mol lower in energy.

At this point, we performed a limited crystal structure prediction (CSP) for paracetamol UPACK[43] (see computational methods section and supplementary information (SI) for details). Similar to our previous work,[5] the GAFF parameter set was used to generate *Z*' = 2 structures in a series of space groups identified as possible matches to the indexed PXRD data. For paracetamol **VII**, these space groups included *P*2$_1$2$_1$2, and *P*222, as well as the initially assigned *P*2$_1$2$_1$2$_1$ and *Pna*2$_1$ due to the relaxed structure identified above. Details of the CSP search can be found in the methods section and in the Supporting Information (SI). In the CSP results, we identified several *Z*' = 2 structures with lattice constants within 0.5 Å of the observed values and energies <10 kJ/mol above the most stable form. The best match was identified in the first 1000 structures for a *Pna*2$_1$ *Z*' = 2 search that was slightly biased to set *a* as the long axis. The four lowest energy structures

were selected for further optimization using density functional theory (DFT) see computational methods section and SI for computational details.

The coordinates from the DFT-optimized structure with the lowest energy ($Pna2_1$, Z = 8, Z' = 2) were chosen for refinement against the PXRD data. Even without refining atomic coordinates, this model produced a reasonably good fit to experimental data (R_p = 2.70 %, R_{wp} = 3.71%, R_{exp} = 2.76 %, gof = 0.787). Next, the molecular geometry was restrained while the orientations, translations, and ψ_1 and ψ_2 torsion angles (Scheme 1) of both independent molecules were refined. This provided an excellent fit with R_p = 1.52 %, R_{wp} = 2.03 %, R_{exp} = 2.74 %, gof = 0.741 (Figure 7). Based on the comparison 20-molecule clusters in COMPACK,[44] this final structure for paracetamol **VII** has a root mean-square deviation (RMSD) of 0.07 Å from the DFT-optimized structure generated by our specific CSP search and 0.101 Å from structure_9 of Neumann and Perrin.[40] The final cif file (see SI) was deposited at the CCDC (ref code 1902047).

Additional diffraction data were collected for the same sample and experimental setup between 100 K and 379 K (-173 to 106 °C). Above 106 °C, the sample converted to **I**. All structures were successfully fit to the same model, R_{wp} < 3 %, indicating that the structure remains unchanged throughout this temperature range. The unit cell dimensions monotonically increase with temperature, with a changing much less in comparison to b and c (Figure 8).

The paracetamol molecule (Scheme 1) is almost flat with ψ_1 = 12° calculated in the gas phase.[45] Based on all ambient pressure crystal structure determinations available in the Cambridge Structure Database, the torsion angles in **I** vary from ψ_1 = 20.19 – 23.49° and ψ_2 = 1.33 – 4.78°. These angles are smaller in **II** with ψ_1 = 16.27 – 18.93° and ψ_2 = 0.14 – 1.52°. In **III** and **VI**, there are two and four independent molecules, respectively, with ψ_1 and ψ_2 varying between 6.64 – 35.63° and 3.21 – 29.92°, respectively. However, since these crystal structures were solved from powder diffraction data, the reliability of these parameters is hard to judge. In **VII** there are two independent molecules with ψ_1 = 13.50 and 22.48° and ψ_2 = 0.22 and 4.00°, respectively, which are similar to the torsion angles measured in **I** and **II**. From the CSP results, we note that the structure most closely related to paracetamol **VII** has a different orientation for one half of all phenyl rings and is only slightly higher in energy. This type of packing may be present in small amounts, but our data does not allow us to identify this disorder.

The crystal structures of paracetamol are held together by NH···O and OH···O hydrogen bonds. In all previously solved structures (**I**, **II**, **III**, and **VI)**, molecules linked by hydrogen bonds to form

layers (Figure 9). These layers are strongly corrugated in **I** and almost flat in all other structures. Two independent molecules in **III** and **VI** arrange as parallel alternating layers. In **VII**, however, two independent molecules form interpenetrating frameworks that are not connected to one another by hydrogen bonds. We note that for the two other low energy *Pna*2$_1$ candidates with similar unit cells identified by CSP, the relative orientation of these networks differs from the observed **VII**. However, in all four structures, molecular packing similarities along *b* and *c* readily explain the low birefringence observed along *a* in polarized light micrographs (Figure 1c).

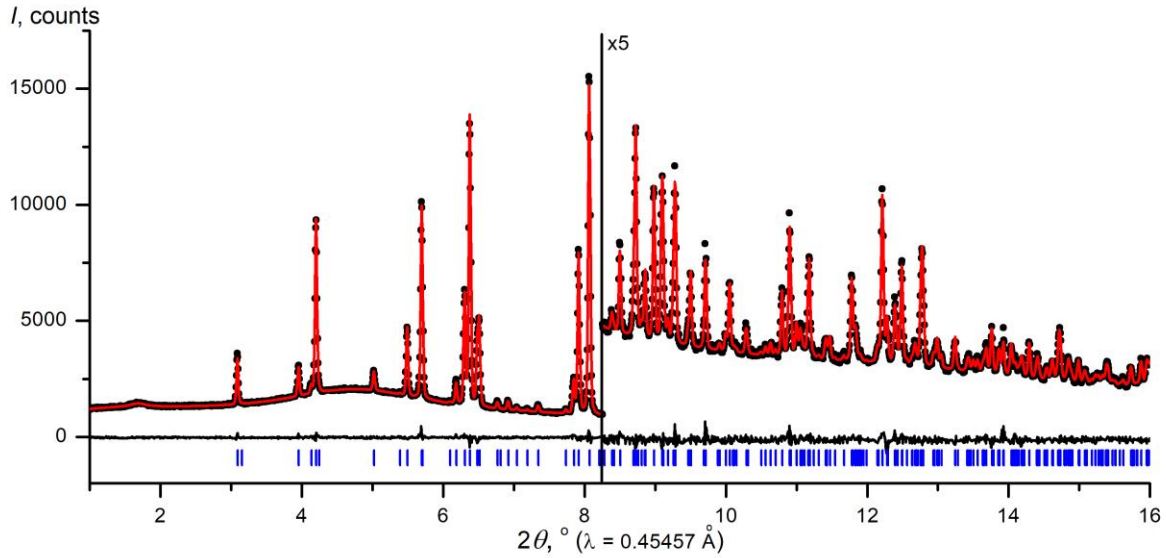

Figure 7. Rietveld refinement of synchrotron powder diffraction data for paracetamol **VII**. The data were collected on the 17-BM beamline at the APS at a wavelength of 0.45457 Å and at 200 K. Observed intensities are displayed as black crosses, while calculated intensities is plotted as a red line. Blue ticks are reflection positions. The lower trace shows the difference curve.

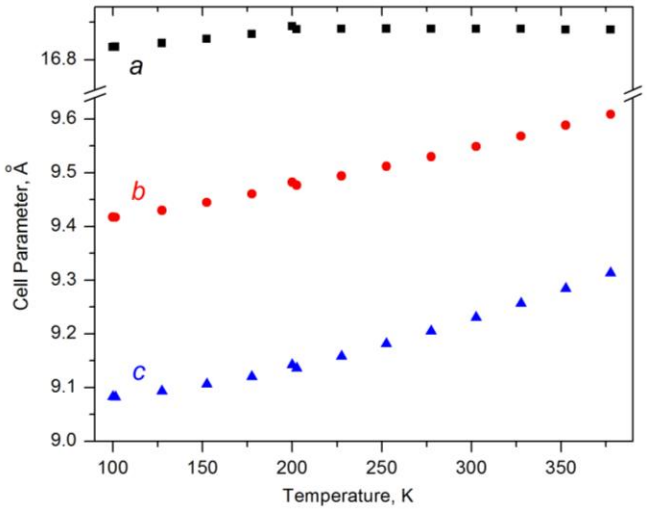

Figure 8. Unit cell dimensions of **VII** as a function of temperature.

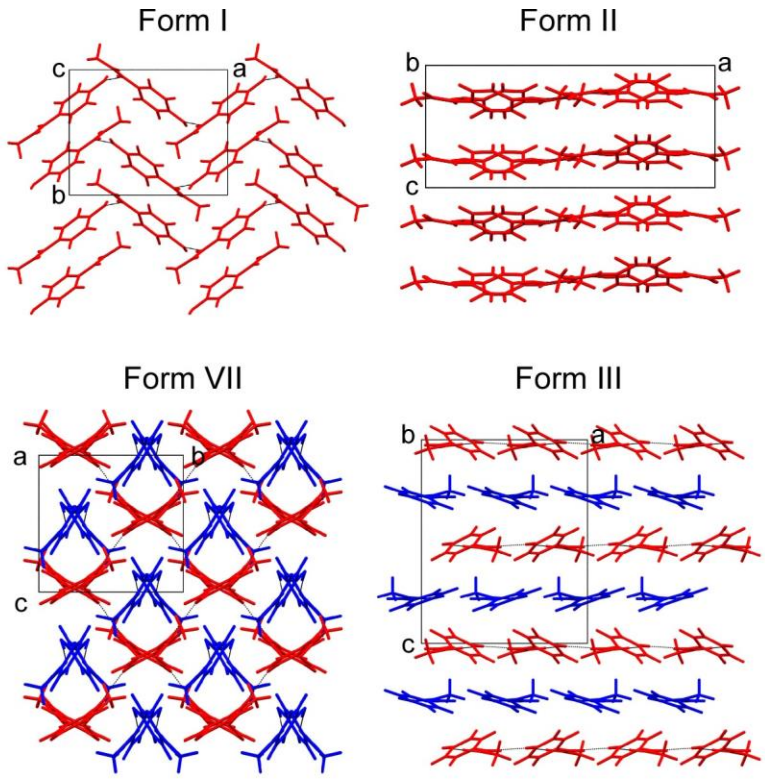

Figure 9. Crystal structures of paracetamol **I** ($P2_1/a$ setting), **II** (*Pbca* setting), **III** ($Pca2_1$ setting), and **VII**, with symmetry inequivalent molecules represented in different colors. Layers in **I**, **II**, and **III** are perpendicular to the plane of the figure.

PARACETAMOL VIII AND IX

Only one diffraction pattern of **VIII** was collected (Figure 10a) because this phase appears infrequently. It exhibits four unique reflections. Unfortunately, the pattern is contaminated by **II** which nucleated on the diffractometer stage via fast polymorph conversion. Although unique reflections observed in **VIII** (12.0, 14.0, 16.2, and 22.9° for Cu *K*α radiation) cannot be explained by the diffraction patterns of **I**, **II**, **III**, and **VII**, they do fit to **IX**. The poor quality of this data precludes distinction between **VIII** and **IX**. Nevertheless, we are confident that this sample represents **VIII**, not **IX**, because it exhibits a distinct morphology (Figure 1e *vs.* 1g, Table 2), is more stable (no transformation was observed upon contact with **III** even after four days at room temperature and sometimes at other temperatures up to 80 °C), produces a unique Raman spectrum (Figure 4), and expresses a much smaller growth rate at 80 °C (Figure 3b). Thus, the occurrence of reflections at similar positions may indicate structural similarities between **VIII** and **IX**.

The powder X-ray diffraction pattern of **IX** was collected at -50 °C using a Bruker SMART APEXII diffractometer (Figure 10b). Because this form is highly metastable, the entire process from sample preparation to data collection was performed under a cold, dry nitrogen flow. The quality of PXRD data precludes direct solution of the crystal structure or even determination of the unit cell dimensions, however, we were able to conclude that one lattice constant may be close to 14.5 Å and another to 25 Å. As no suitable candidate was found in the forms predicted by Neumann and Perrin,[40] we performed our own CSP search using the general Amber force field (GAFF)[42] in the UPACK software package[43] (details can be found in the SI). An extensive search for Z' = 1 and 2 structures in the 13 common space groups, along with those identified as possibilities for **VII**, did not yield any structures matching the observed diffraction pattern for **IX**. The lack of any reasonable candidate structures suggests that the structure of **IX** is likely $Z' > 2$.

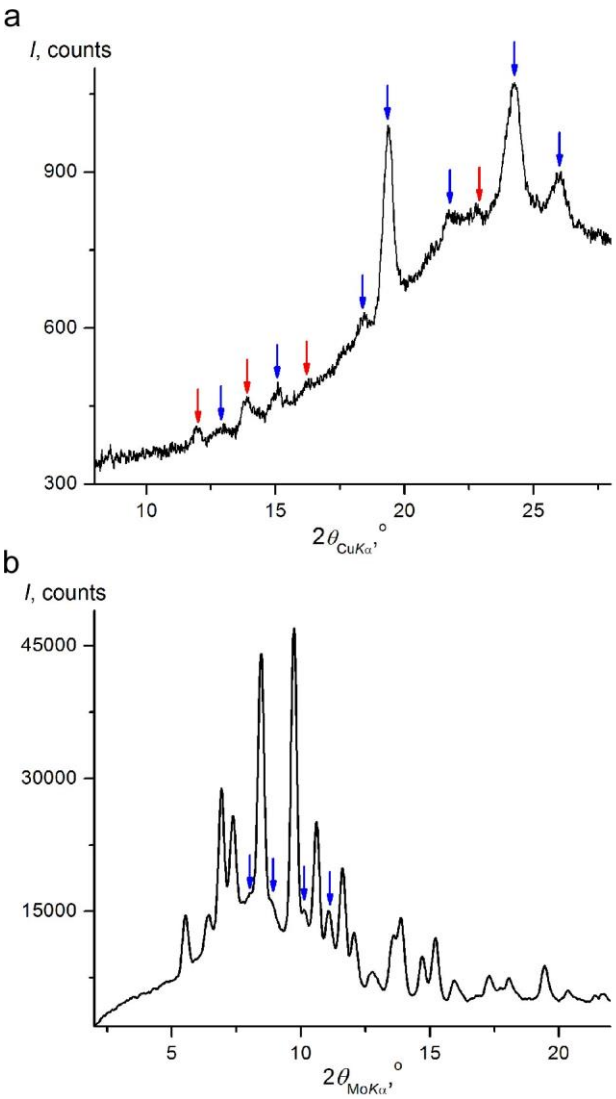

Figure 10. (a) Powder diffraction pattern of **VIII** collected at room temperature with Bruker AXS D8 DISCOVER GADDS microdiffractometer. Red arrows denote positions of unique reflections of **VIII**, while blue arrows are reflections of **II**. (b) Powder diffraction pattern of **IX** collected at -50 °C with Bruker SMART APEXII diffractometer. Blue arrows correspond to possible minor contamination by **II**.

CONCLUSIONS

This work is a case study in using melt crystallization in conjunction with polarized light optical microscopy in the characterization of polymorphs for one of the most well-studied molecular crystals. We identified three new ambient polymorphs of paracetamol and solved the crystal structure of one of them. In addition, we have described growth and phase transformations in the system, discovered a rare glass-to-crystal growth mode for two polymorphs, and found spontaneous helical twisting for two polymorphs.

EXPERIMENTAL

A few mg of paracetamol (Sigma-Aldrich, >98 %) were placed between a microscope slide and a glass cover slip and melted on a Kofler bench at *ca*. 200 °C. The samples were subsequently cooled to room temperature and crystallized between 50 and 120 °C, or in a refrigerator at 0.5 and 8 °C. Some samples were re-melted and crystallized on a hot stage (Model FP90, Mettler-Toledo) at 24-169 °C. Polarized light micrographs were made with an Olympus BX50 microscope equipped with a digital camera. Relative humidity (RH) was determined using the humidity sensor (Electro-Tech Systems, Inc.).

X-ray diffraction (XRD) patterns were collected on a Bruker D8 DISCOVER GADDS microdiffractometer equipped with a VÅNTEC-2000 two-dimensional detector and a 0.5 mm MONOCAP collimator (Cu *K*α radiation). The data collection was performed in reflection mode either on an as-grown crystalline film on a glass slide with the cover glass removed or on powder detached from the glass slide and mounted on a silicon wafer with a small amount of vacuum grease.

The powder diffraction pattern of **IX** was collected on a Bruker SMART APEXII single crystal diffractometer (Mo *K*α radiation, λ = 0.71073 Å) equipped with a two-dimensional CCD detector with the sample-detector distance at 150 mm. The cover slip was detached under a cold, dry nitrogen stream (*T* = -50 °C controlled by an Oxford Cryosystems 700+ Cooler). The marked area containing only form **IX** was kept under the cold nitrogen stream, a thin layer of immersion oil

was applied to coat the area, and the powder in the area was carefully scraped with a sharp needle. The powder was piled up into a small ball with a dimension of *ca*. 300 μm and attached to a Hampton Nylon loop, which was mounted on the goniometer head of the diffractometer for measurement at -50 °C.

High signal-to-noise ratio synchrotron powder diffraction data of **VII** were collected on the 17-BM beamline of the Advanced Photon Source, Argonne National Laboratory, at a wavelength of 0.45457 Å using a PerkinElmer PE1621 area detector. Paracetamol **VII** was prepared by a similar procedure as **IX** but at ambient conditions. The powder patterns were collected first at 200 K and then from 100 to 423 K at a temperature interval of *ca*. 25 K. In all cases the temperature was controlled using an Oxford 700+ Cooler.

Raman spectra were collected with a Thermo Scientific DXR Raman microscope (laser wavelength 532 nm, laser power 8 mW, high-resolution grating, resolution cm^{-1}) from an as-grown crystalline film on a glass slide covered with cover glass.

COMPUTATIONAL METHODS

The CSP approach for paracetamol included a $Z' = 1$ or 2 search in the 13 common space groups (>50,000 structures each) and an additional $Z' = 2$ search in the $P2_12_12$, $P2_122$, and $P222$ space groups. Structures were generated using a rigid body random search algorithm in the UPACK program suite[43] with each molecule described using the general Amber force field (GAFF).[42] Atomic point charges for the classical force field were determined using the restricted electrostatic potential (RESP) charge assignment scheme[46] using RHF/6-31G*//MP2/6-31G* in Gaussian09.[47] A summary of the CSP results and the resulting energy vs. molecular volume plot for the 500 most stable predicted forms are included in the Supporting Information.

For each structure with simulated PXRD patterns similar to the observed data, the atomic coordinates and cell vectors were optimized using the Gaussian and plane wave (GPW) scheme[48] of the QUICKSTEP package[49] in CP2K v. 2.6.2[50] Each system was optimized using the PBE exchange-correlation functional [51] with the D3(BJ) dispersion correction. [52, 53] For these calculations, the TZVP-MOLOPT-GTH basis set and corresponding GTH pseudopotentials[54,55] were used with an energy cutoff of 900 Ry. Additional computational details can be found in the Supporting Information.

ACKNOWLEDGEMENTS

This work was primarily supported by the New York University Materials Research Science and Engineering Center (MRSEC) program of the National Science Foundation under award number DMR-1420073. Funding support was also provided by the National Science Foundation (grant DMR-1608374). This work was supported by computational resources provided by High Performance Computing resources at New York University. The authors acknowledge the NSF Chemistry Research Instrumentation and Facilities Program (CHE-0840277) for the powder microdiffractometer. This research used resources of the Advanced Photon Source, a U.S. Department of Energy (DOE) Office of Science User Facility operated for the DOE Office of Science by Argonne National Laboratory under contract no. DE-AC02-06CH11357.

REFERENCES

1 Morissette, S. L.; Almarsson, O.; Perterson, M. L.; Remenar, J. F.; Read, M. J.; Lemmo, A. V.; Ellis, S.; Cima, M. J.; Gardner, C. R. High-throughput crystallization: polymorphs, salts, co-crystals and solvates of pharmaceutical solids. *Adv. Drug Delivery Rev.* **2004**, *56*, 275-300.

2 Shtukenberg, A. G.; Gunn, E.; Yu, L.; Kahr, B. Glass-crystal growth mode for testosterone propionate. *Cryst. Growth Des*. **2011**, *11*, 4458-4462.

3 Zhu, Q.; Shtukenberg, A. G.; Carter, D. J.; Yu, T.-Q.; Yang, J.; Chen, M.; Raiteri, P.; Oganov, A. R.; Pokroy, B.; Polishchuk, I.; Bygrave, P. J.; Day, G. M.; Rohl, A. L.; Tuckerman, M. E.; Kahr, B. Resorcinol crystallization from the melt: A new ambient phase and new "riddles." *J. Am. Chem. Soc*. **2016**, *138*, 4881-4889.

4 Shtukenberg, A. G.; Hu, C. T.; Zhu, Q.; Schmidt, M. U.; Xu, W.; Tan, M.; Kahr, B. The third ambient aspirin polymorph. *Cryst. Growth Des*. **2017**, *17*, 3562–3566.

5 Shtukenberg, A. G.; Zhu, Q.; Carter, D. J.; Vogt, L.; Hoja, J.; Schneider, E.; Song, H.; Pokroy, B.; Polishchuk, I.; Tkatchenko, A.; Oganov, A. R.; Rohl, A. L.; Tuckerman, M. E.; Kahr, B. Powder diffraction and crystal structure prediction identify four new coumarin polymorphs. *Chem. Sci*. **2017**, *8*, 4926-4940.

6 Yang, J.; Hu, C. T.; Zhu, X.; Zhu, Q.; Ward, M. D.; Kahr, B. DDT Polymorphism and the lethality of crystal forms. *Angew. Chem*. **2017**, *129*, 10299-10303.

7 Haisa, M.; Kashino, S.; Kawai, R.; Maeda, H. The monoclinic form of *p*-hydroxyacetanilide. *Acta Crystallogr. B* **1976**, *32*, 1283-1285.

8 Haisa, M.; Kashino, S.; Maeda, H.: The orthorhombic form of *p*-hydroxyacetanilide. *Acta Crystallogr*. *B* **1974**, *30*, 2510-2512.

9 Perrin, M.-A.; Neumann, M. A.; Elmaleh, H.; Zaske, L. Crystal structure determination of the elusive paracetamol Form III. *Chem. Comm*. **2009**, *22*, 3181-3183.

10 Smith, S. J.; Bishop, M. M.; Montgomery, J. M.; Hamilton, T. P.; Vohra, Y. K. Polymorphism in paracetamol: Evidence of additional forms IV and V at high pressure. *J. Phys. Chem. A* **2014**, *118*, 6068-6077.

11 Reiss, C. A.; van Mechelen, J. B.; Goubitzc, K.; Peschar, R. Reassessment of paracetamol orthorhombic Form III and determination of a novel low temperature monoclinic Form III-m from powder diffraction data. *Acta Crystallogr. C* **2018**, *74*, 392-399.

12 Di Martino, P.; Conflant, P.; Drache, M.; Huvenne, J.-P.; Guyot-Hermann, A.-M. Preparation and physical characterization of forms II and III of paracetamol. *J. Therm. Anal*. **1997**, *48*, 447-458.

13 Qi, S.; Avalle, P.; Saklatvala, R.; Craig, D. Q. M. An investigation into the effects of thermal history on the crystallisation behaviour of amorphous paracetamol. *Eur. J. Pharm. Biopharm*. **2008**, *69*, 364-371.

14 Burley, J. C.; Duer, M. J.; Stein, R. S.; Vrcelj, R. M. Enforcing Ostwald's rule of stages: Isolation of paracetamol forms III and II. *Eur. J. Pharm. Sci*. **2007**, *31*, 271-276.

15 Rivalta, A.; Salzillo, T.; Venuti, E.; Della Valle, R. G.; Sokolovič, B.; Werzer, O.; Brillante, A. Bulk and surface-stabilized structures of paracetamol revisited by Raman confocal microscopy. *ACS Omega* **2018**, *3*, 9564-9571.

16 Wang, S.-L.; Lin, S.-Y.; Wei, Y.-S. Transformation of Metastable Forms of Acetaminophen Studied by Thermal Fourier Transform Infrared (FT-IR) Microspectroscopy. *Chem. Pharm. Bull*. **2002**, *50*, 153-156.

17 Szelagiewicz, M.; Marcolli, C.; Cianferani, S.; Hard, A. P.; Vit, A.; Burkhard, A.; von Raumer, M.; Hofmeier, U. Ch.; Zilian, A.; Francotte, E.; Schenker, R. In situ characterization of polymorphic forms. The potential of Raman techniques. *J. Therm. Anal. Calorim.* **1999**, *57*, 23-43.

18 Sibik, J.; Sargent, M. J.; Franklin, M.; Zeitler, J. A. Crystallization and phase changes in paracetamol from the amorphous solid to the liquid phase. *Mol. Pharm.* **2014**, *11*, 1326-1334.

19 de Wet, F. N.; Gerber, J. J.; Lotter, A. P.; Van Der Watt J. G.; Dekker, T. G. A Study of the changes during heating of paracetamol. *Drug Dev. Ind. Pharm*. **1998**, *24*, 447-453.

20 Nanubolu, J. B.; Burley, J. C. Investigating the recrystallization behavior of amorphous paracetamol by variable temperature Raman studies and surface Raman mapping. *Mol. Pharm*. **2012**, *9*, 1544-1558.

21 Boldyreva, E. V.; Drebushchak, V. A.; Paukov, I. E.; Kovalevskaya, Y. A.; Drebushchak, T. N. DSC and adiabatic calorimetry study of the polymorphs of paracetamol. *J. Therm. Anal. Calorim*. **2004**, *77*, 607-623.

22 Gobbo, G.; Bellucci, M. A.; Tribello, G. A.; Ciccotti, G.; Trout, B. L. Nucleation of molecular crystals driven by relative information entropy. *J. Chem. Theory Comput*. **2018**, *14*, 959-972.

23 Rengarajan, G. T.; Enke, D.; Steinharta, M.; Beiner, M. Size-dependent growth of polymorphs in nanopores and Ostwald's step rule of stages. *PhysChemPhys* **2011**, *13*, 21367-21374.

24 Oparin, R. D.; Moreau, M.; De Walle, I.; Paolantoni, M.; Idrissi, A.; Kiselev M. G. The interplay between the paracetamol polymorphism and its molecular structures dissolved in supercritical CO_2 in contact with the solid phase: In situ vibration spectroscopy and molecular dynamics simulation analysis. *Eur. J. Pharm. Sci*. **2015**, *77*, 48-59.

25 Kauffman, J. F.; Batykefer, L. M.; Tuschel, D. D. Raman detected differential scanning calorimetry of polymorphic transformations in acetaminophen. *J. Pharm. Biomed. Anal.* **2008**, *48*, 1310-1315.

26 Kolesov, B. A.; Mikhailenko, M. A.; Boldyreva, E. V. Dynamics of the intermolecular hydrogen bonds in the polymorphs of paracetamol in relation to crystal packing and conformationaltransitions: a variable-temperature polarized Raman spectroscopy study. *Phys. Chem. Chem. Phys.* **2011**, *13*, 14243-14253.

27 Shtukenberg, A.; Punin, Yu.O.; Gunn, E.; Kahr, B. Spherulites. *Chem. Rev*. **2012**, *112*, 1805-1838.

28 Xi, H.; Sun, Y.; Yu, L. Diffusion-controlled and diffusionless crystal growth in liquid o-terphenyl near its glass transition temperature. *J. Chem. Phys*. **2009**, *130*, 094508.

29 Sun, Y.; Xi, H.; Chen, S.; Ediger, M. D.; Yu, L. Crystallization near glass transition: Transition from diffusion-controlled to diffusionless crystal growth studied with seven polymorphs. *J. Phys. Chem. B* **2008**, *112*, 5594-5601.

30 Greet, R. J.; Turnbull, D. Glass transition in *o*-terphenyl. *J. Chem. Phys*. **1967**, *46*, 1243-1251.

31 Musumeci, D.; Powell, C. T.; Ediger, M. D.; Yu, L. Termination of Solid-State Crystal Growth in Molecular Glasses by Fluidity *J. Phys. Chem. Lett*. **2014**, *5*, 1705-1710.

32 Powell, C. T.; Xi, H.; Sun, Y.; Gunn, E.; Chen, Y.; Ediger, M. D.; Yu, L. Fast crystal growth in o-terphenyl glasses: a possible role for fracture and surface mobility. *J. Phys. Chem. B* **2015**, *119*, 10124-10130.

33 Bernauer, F. *"Gedrillte" Kristalle*; Gebruder Bornträger: Berlin, 1929.

34 Shtukenberg, A. G.; Punin, Yu. O.; Gujral, A.; Kahr, B. Growth actuated bending and twisting of crystals. *Angew. Chem. Int. Ed*. **2014**, *53*, 672-699.

35 Shtukenberg, A.; Gunn, E.; Gazzano, M.; Freudenthal, J.; Camp, E.; Sours, R.; Rosseeva, E. Kahr, B. Bernauer's bands. *ChemPhysChem* **2011**, *12*, 1558-1571.

36 Shtukenberg, A.; Freudenthal, J.; Kahr, B. Reversible twisting during helical hippuric acid crystal growth. *J. Am. Chem. Soc.* **2010**, *132*, 9341-9349.

37 Cui, X.; Nichols, S.; Arteaga, O.; Freudenthal. J.; Paula, F.; Shtukenberg, A. G., Kahr, B. Dichroism in helicoidal crystals. *J. Am. Chem. Soc*. **2016**, *138*, 12211–12218.

38 Shtukenberg, A. G.; Gujral, A.; Rosseeva, E.; Cui, X.; Kahr, B. Mechanics of twisted hippuric acid crystals untwisting as they grow. *CrystEngComm* **2015**, *17*, 8817-8824.

39 Le Bail, A. Monte Carlo indexing with McMaille. *Powder Diffraction* **2004**, *19*, 249-254.

40 Neumann, M. A.; Perrin, M.-A. Can crystal structure prediction guide experimentalists to a new polymorph of paracetamol? *CrystEngComm* **2009**, *11*, 2475-2479.

41 Bruker AXS. *TOPAS V4.2: General profile and structure analysis software for powder diffraction data.* Bruker AXS, Karlsruhe, Germany, 2008.

42 Wang, J.; Wolf, R. M.; Caldwell, J. W.; Kollman, P.A.; Case, D. A. Development and testing of a general amber force field. *J. Comput. Chem.* **2004**, *25*, 1157-1174.

43 van Eijck, B. P.; Kroon, J. UPACK program package for crystal structure prediction: force fields and crystal structure generation for small carbohydrate molecules. *J. Comput. Chem.* **1999**, *20*, 799-812.

44 Chisholm, J. A.; Motherwell, S. COMPACK: A program for identifying crystal structure similarity using distances. *J. Appl. Crystallogr*. **2005**, *38*, 228–231.

45 Beyer, T.; Price, S. L. The errors in lattice energy minimisation studies: Sensitivity to experimental variations in the molecular structure of paracetamol. *CrystEngComm* **2000**, *34*, 1-8.

46 Bayly, C. I.; Cieplak, P.; Cornell, W.; Kollman, P. A. A well-behaved electrostatic potential based method using charge restraints for deriving atomic charges: The RESP model. *J. Phys. Chem.* **1993**, *97*, 10269-10280.

47 Frisch, M. J.; Trucks, G. W.; Schlegel, H. B.; Scuseria, G. E.; Robb, M. A.; Cheeseman, J. R.; Scalmani, G.; Barone, V.; Petersson, G. A.; Nakatsuji, H.; Li, X.; Caricato, M.; Marenich, A.; Bloino, J.; Janesko, B. G.; Gomperts, R.; Mennucci, B.; Hratchian, H. P.; Ortiz, J. V.; Izmaylov, A. F.; Sonnenberg, J. L.; Williams-Young, D.; Ding, F.; Lipparini, F.; Egidi, F.; Goings, J.; Peng, B.; Petrone, A.; Henderson, T.; Ranasinghe, D.; Zakrzewski, V. G.; Gao, J.; Rega, N.; Zheng, G.; Liang, W.; Hada, M.; Ehara, M.; Toyota, K.; Fukuda, R.; Hasegawa, J.; Ishida, M.; Nakajima, T.; Honda, Y.; Kitao, O.; Nakai, H.; Vreven, T.; Throssell, K.; Montgomery, Jr., J. A.; Peralta, J. E.; Ogliaro, F.; Bearpark, M.; Heyd, J. J.; Brothers, E.; Kudin, K. N.; Staroverov, V. N.; Keith, T.; Kobayashi, R.; Normand, J.; Raghavachari, K.; Rendell, A.; Burant, J. C.; Iyengar, S. S.; Tomasi, J.; Cossi, M.; Millam, J. M.; Klene, M.; Adamo, C.; Cammi, R.; Ochterski, J. W.; Martin, R. L.; Morokuma, K.; Farkas, O.; Foresman, J. B.; Fox, D. J. GAUSSIAN09. Gaussian Inc., Wallingford, CT, USA, 2009.

48 Lippert, G.; Hutter, J.; Parrinello, M. A hybrid Gaussian and plane wave density functional scheme. *Mol. Phys.* **1997**, *92*, 477-488.

49 VandeVondele, J.; Krack, M.; Mohamed, F.; Parrinello, M.; Chassaing, T.; Hutter, J. QUICKSTEP: Fast and accurate density functional calculations using a mixed Gaussian and plane waves approach. *Comput. Phys. Commun.* **2005**, *167*, 103-128.

50 Hutter, J.; Iannuzzi, M.; Schiffmann, F.; VandeVondele, J. CP2K: Atomistic simulations of condensed matter systems. *WIREs Comput. Mol. Sci.* **2014**, *4*, 15-25.

51 Perdew, J. P.; Burke, K.; Ernzerhof, M. Generalized gradient approximation made simple. *Phys. Rev. Lett.* **1996**, *77*, 3865-3868.

52 Grimme, S.; Antony, J.; Ehrlich, S.; Krieg, H. A consistent and accurate *ab initio* parametrization of density functional dispersion correction (DFT-D) for the 94 elements H-Pu. *J. Chem. Phys.* **2010**, *132*, 154104.

53 Grimme, S.; Ehrlich, S.; Goerigk, L. Effect of the damping function in dispersion corrected density functional theory. *J. Comput. Chem.* **2011**, *32*, 1456-1465.

54 Goedecker, S.; Teter, M.; Hutter, J. Separable dual-space Gaussian pseudopotentials. *Phys. Rev. B: Condens. Matter* **1996**, *54*, 1703-1710.

55 Krack, M. Pseudopotentials for H to Kr optimized for gradient-corrected exchange-correlation functionals. *Theor. Chem. Acc.* **2005**, *114*, 145-152.